Analysis of End Effects in a Spherical Induction Motor with Shell-Like stator

André Filipe Mendonça Sá Roque
andre.roque@tecnico.ulisboa.pt

Instituto Superior Técnico, Lisboa, Portugal

November 2016

Abstract

The general equation and a particular solution to the magnetic field inside the air gap of a shell-like stator induction motor with spherical rotor is to be found. In this machine's geometry, a discontinuity of the stator iron core exists, creating a complex profile for the magnetic field inside the air gap, besides the travelling wave typically found. This phenomenon is called the end effects. In order to study these effects, previous studies of end effects in linear induction motors with Field Theory were used as a basis, whose geometry also shares the stator iron core discontinuity. Hence, a link between the end effects of the two geometries was sought, keeping in mind that the analysis for the spherical rotor was made in cylindrical coordinates, while Cartesian coordinates were used for the linear motor. A model was found for the magnetic field inside the air gap, and its parameters were tested for various motors configurations, such as varying air gaps, secondary sheet resistivity, rotor radiuses and power supply frequencies. Thrust curves were obtained and the impact of the end effects on motor performance was found, making a distinction between high speed and low speed motors, whose motor performance impact due to the end effect varies differently. It was possible to find ways to minimize the impact of the end effect on motor's performance from the variation of the model's parameters with various motor configurations.

Keywords: End Effects, Spherical Rotor, Induction Motor, Shell-Like Stator, Magnetic Field

1. Introduction

The induction motor with spherical rotor and shell-like stator is proposed by this work's supervisor [1], depicted in figure 1. The functioning of the motor is based on the typical rotary induction motors with cylindrical rotors. However, by creating a spherical rotor and superposing two perpendicular primary windings, it is possible to control the rotor's motion in two axis, creating an omnidirectional machine.

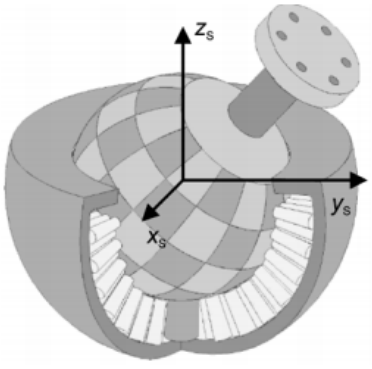

Figure 1: Spherical rotor visualization as per [2].

The shell-like stator serves the purpose of inducing currents in the rotor's conductive sheet, creating thrust and hence motion. A fully enclosed shell would have the best performance, as more current would be fed into the stator and hence to the rotor. However, it would also inhibit the degree in each of the two axis in which the rotor can rotate freely, as there is a need to attach an axis to the rotor in order to retrieve the mechanical energy related to the motor's movement. Therefore, fully enclosed stators have little applications.

The end effects have been subject of study ever since the development of linear induction motors. Various authors have reported the effects over the years, and experiments were first conducted in Japan [3]. These effects are often divided in two categories [4]: longitudinal end effects and transverse end effects.

The longitudinal end effects occur due to the discontinuity of the primary iron core, that is to say, the stator, in the direction of the movement of the motor, creating a turbulent magnetic field inside the air gap. These end effects are also divided in two categories: static and dynamic. The static end

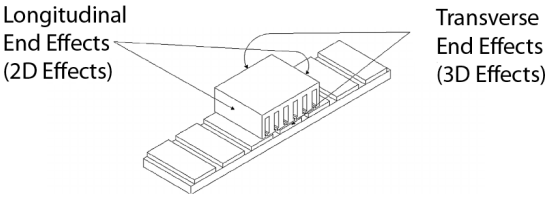

Figure 2: Longitudinal and transverse end effects representation [5].

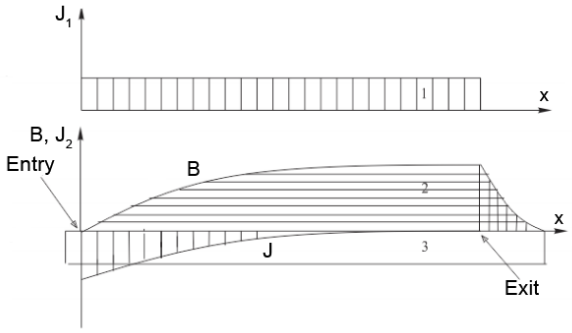

Figure 3: Dynamic end effects representation - primary current density J_1 and corresponding secondary current density J_2 and magnetic field in the air gap [4].

effects occur independently of the speed of the motor, and are influenced only by the geometry of the motor, namely, the primary windings distribution. The dynamic end effects are dependent on the motor speed, being more prevalent as the motor speed increases, and are generally associated with the study of the end effects as a whole.

The connection between linear induction motors and the novel spherical rotor motors lies in the existence of end effects, since having a non fully-enclosed stator in a spherical rotor motor will create discontinuities in the primary iron core, very similarly to the ones observed in the linear induction motor. As such, reduction of performance is also verified in the spherical rotor motors due to the end effects, and should be analysed in order to better understand the influence of the motor parameters in reduced performance. Therefore, using as a basis previous literature on the study of end effects in linear induction motors, a model for the end effects in the spherical rotor motor with shell-like stator is to be found.

2. Background

The dynamic end effects occur as soon as the motor acquires speed [6]. To understand this phenomenon, a graphical explanation is required.

Considering a small domain in the secondary not under the influence of the primary, that is to say, away from the air gap, it is reasonable to say that both the magnetic field and current in this domain is zero. As this domain approaches the entry of the air gap, a sudden variation of magnetic field is verified, being provided by the primary. The secondary will respond opposing this sudden variation of magnetic field in this domain. Therefore, as this domain in the secondary starts to enter the air gap, instead of instantaneously raising its magnetic field to the one seen in the air gap, a damped increase of the magnetic field in this domain is seen. This damping has a time constant that is related to the characteristics of the iron in the secondary, in order to satisfy the continuity of the magnetic field along every domain of the secondary [6].

At the exit end, the opposite effect occurs. If the air gap is long enough, near the exit, there is no more damping of the magnetic field in the domain considered. Therefore, up until the end of the air gap, the magnetic field in this domain should have stabilised. As this domain exits the air gap, there is once again a sudden variation of the magnetic field and induced current, because it is no longer under the influence of the primary. This time, however, the domain will try to maintain its continuity by having a damped decrease of the magnetic field outside the air gap, creating a "tail" as if it were of magnetic field. This damping's time constant is different from the first damping, as it is no longer under the primary ferromagnetic core [6].

Analysis on end effects is mostly done through Field Theory [3], [7], [8]. The magnetic circuit can be analysed through Ampère's Law and Electromotive Force, resulting in a differential equation for the magnetic field $\mathbf{B}$ inside the air gap.

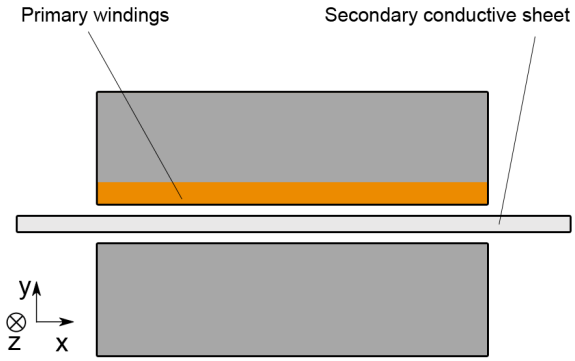

Figure 4: One-dimensional model for the linear induction motor.

Many approaches may be taken. The simplest is based on the assumption that the magnetic field inside the air gap is constant along the y coordinate, as per figure 4. Therefore, only a solution for $\mathbf{B_y}$

is to be found, which will be a function of x. This is called the one-dimensional model, which will be the one which this works delves into. For the one-dimensional approach, there are still many different considerations that can be taken into account. It is possible to create a second, third or even fourth order system [7].

The second order system is a simple application of both Ampère's Law and Electromotive Force in a small domain, while making no extra considerations, resulting in a second order differential equation. Therefore, two roots exist for the transient term, or rather, the total solution is the superposition of two transient magnetic fields plus the steady state solution. These two transient magnetic fields, which will be studied in detail further ahead, are related to the necessity of continuity of magnetic flux in the extremities of the primary iron core, both entry and exit ends. The amplitudes of these transient waves can only be obtained through a set of boundary conditions, defined according to the geometry considered.

One boundary condition often used is the flux conservation, meaning that the steady state magnetic field solution, that is to say, the travelling wave created by the primary current density, and the transient magnetic fields, along the air gap length, must add up to zero. Another simple boundary condition is to consider that, outside the air gap, the secondary current density is zero, or in other words, that no magnetic field exists outside the air gap. Studies with the proposed model have shown that this second condition might be too simplistic, and can be corrected by considering that there is magnetic field at a small distance outside the air gap.

3. One Dimensional Model

In traditional cylindrical machines, the rotor is fully enveloped by the stator, meaning that every point on the surface of the rotor is subject at all times, in steady state, to a magnetic field provided by the stator. A shell-like stator introduces a discontinuity of the magnetic field from the standpoint of view of the rotor.

A series of physical entities will be introduced. Firstly, it is considered that the radius of the motor is r_s for the stator and r_r for the rotor. Equivalent conductive sheet's widths will be considered. That is to say, for the primary winding, a very thin conductive sheet will be considered instead. The same will be considered for the secondary sheet, and the real width will only be considered for the actual current densities. Therefore, the equivalent air gap is given by $g = r_s - r_r + d_s + d_r$.

The primary current density is considered to be $\mathbf{j_1}$, while the secondary current density is $\mathbf{j_2}$. Finally, it is considered that the angle of the shell-like stator is β, that is to say, the primary envelopes the secondary in β radians.

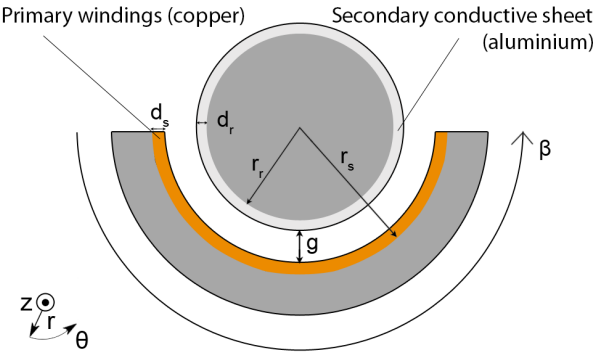

Figure 5: System coordinates.

3.1. Second order system

Considering that the magnetic field is dependent of only the θ coordinate, meaning that $\mathbf{B}$ is constant along the r coordinate, only a solution for $\mathbf{B_r}(t, \theta)$ is to be found. This can be a good approximation if the air gap is small enough. Applying Ampère's law in the integral form in this cylindrical geometry results in:

$$\int_{r_r}^{r_s} \mathbf{H}(\theta = \theta_1)dr - \int_{r_r}^{r_s} \mathbf{H}(\theta = \theta_2)dr = \int_{\theta_1}^{\theta_2} \mathbf{j_1} r_s d\theta + \int_{\theta_1}^{\theta_2} \mathbf{j_2} r_r d\theta. \tag{1}$$

The resulting application of Ampère's law results in

$$-\frac{\partial \mathbf{B}}{\partial \theta} = \mu_0[\mathbf{j_1}(r_g + 1) + \mathbf{j_2} r_g] \tag{2}$$

where r_g is given by:

$$r_g = \frac{r_r}{g}. \tag{3}$$

The Maxwell-Faraday equation in cylindrical coordinates is given by:

$$\boldsymbol{\epsilon} = -\frac{\partial \mathbf{A}}{\partial t} - \omega_r \frac{\partial \mathbf{A}}{\partial \theta} \tag{4}$$

with ω_r being the rotor speed.

Differentiating the electromotive force expression in order of θ:

$$\frac{\partial \boldsymbol{\epsilon}}{\partial \theta} = -r_r \frac{\partial \mathbf{B}}{\partial t} - \omega_r r_r \frac{\partial \mathbf{B}}{\partial \theta}. \tag{5}$$

3.2. General Equation for the Magnetic Field

The width of the secondary conductor sheet will be considered, resulting in an equivalent secondary conductor resistivity, given by:

$$\rho_s = \frac{\rho}{d_r} \tag{6}$$

where ρ is the rotor's resistivity and d_r is the thickness of the rotor's surface conducting material. Substituting the equation resulting from the electromotive force into the equation resulting from Ampère's law creates the general expression of the model, which can be seen in:

$$\frac{\partial^2 \mathbf{B}}{\partial \theta^2} - \mu_0 \frac{r_g r_r}{\rho_s} \frac{\partial \mathbf{B}}{\partial t} - \mu_0 \frac{r_g r_r \omega_r}{\rho_s} \frac{\partial \mathbf{B}}{\partial \theta} = -\mu_0 \frac{\partial \mathbf{j_1}}{\partial \theta}(r_g + 1). \tag{7}$$

3.3. Solution for the General Equation

In steady-state, it can be assumed that the magnetic field in the air gap is simply a travelling wave. This can be obtained if it is considered that no end-effects occur in the motor. In other words, in typical linear induction motor terms, it is considered that the motor length is infinite. Such notion makes no sense considering the cylindrical coordinates, and as such, a more appropriate analogy would be to consider that the motor length is $\beta = 2\pi$, or that the motor is a typical closed cylindrical rotary induction motor.

It is assumed that the current density in the primary is given by:

$$\mathbf{j_1} = J_1 \exp\left[\jmath(\omega t - k\theta)\right] \tag{8}$$

in which ω is the angular frequency of the power supply and k is the number of pair-poles.

The amplitude J_1 is a real value representing an equivalent amplitude, in which the width of the primary conductive sheet is taking into account. Hence, $J_1 = \frac{J_M}{d_s}$, where J_M is the actual amplitude of the current density. Therefore, the magnetic field expression is given by:

$$\mathbf{B} = \overline{B_s} \exp\left[\jmath(\omega t - k\theta)\right]. \tag{9}$$

Substituting the travelling wave in the general equation for the magnetic field given by equation 7, the amplitude of the travelling wave can be found in:

$$\overline{B_s} = -\frac{\jmath J_1 (r_g + 1) k \mu_0}{k^2 + \jmath \frac{r_g r_r \mu_0}{\rho_s} s\omega}. \tag{10}$$

The slip of the motor s is defined as:

$$s = \frac{\omega - k\omega_r}{\omega}. \tag{11}$$

3.4. Transient Solution

The transient solution can be obtained through the homogeneous equation, meaning equalling the general equation to zero: .

$$\frac{\partial^2 \mathbf{B}}{\partial \theta^2} - \mu_0 \frac{r_g r_r}{\rho_s} \frac{\partial \mathbf{B}}{\partial t} - \mu_0 \frac{r_g r_r \omega_r}{\rho_s} \frac{\partial \mathbf{B}}{\partial \theta} = 0 \tag{12}$$

Solving the general equation through the Fourier Transform, the resulting characteristic equation obtained is:

$$s^2 - \frac{\omega_r r_g r_r \mu_0}{\rho_s} s - \frac{\jmath \omega r_g r_r \mu_0}{\rho_s} = 0 \tag{13}$$

The solutions for the characteristic equation can be found in expression 14 and 15.

$$\overline{s_1} = \frac{\omega_r r_g r_r \mu_0 - \rho_s X}{2\rho_s} - \jmath \frac{Y}{2} \equiv -\frac{1}{\alpha_1} - \jmath k_e \tag{14}$$

$$\overline{s_2} = \frac{\omega_r r_g r_r \mu_0 + \rho_s X}{2\rho_s} + \jmath \frac{Y}{2} \equiv \frac{1}{\alpha_2} + \jmath k_e \tag{15}$$

$$\alpha_1 = \frac{2\rho_s}{\rho_s X - \omega_r r_g r_r \mu_0} \tag{16}$$

$$\alpha_2 = \frac{2\rho_s}{\rho_s X + \omega_r r_g r_r \mu_0} \tag{17}$$

$$k_e = \frac{Y}{2} \tag{18}$$

This will result in a sum of two waves for the transient solution, in the form of:

$$\overline{B_1} \exp\left(\overline{s_1}\theta\right) \exp\left(\jmath\omega t\right) + \overline{B_2} \exp\left(\overline{s_2}\theta\right) \exp\left(\jmath\omega t\right) = \mathbf{B_1} + \mathbf{B_2}. \tag{19}$$

The transient solution shows two waves, $\mathbf{B_1}$ and $\mathbf{B_2}$. The first wave will be called the entry end effect wave, while the second wave will be called the exit end effect wave. The reason for this will become clear when the boundary conditions are defined. The first wave $\mathbf{B_1}$ is related to the discontinuity of the iron core in the vicinity of the entry of the air gap, in relation to the rotating direction in θ of the motor. Similarly, the wave $\mathbf{B_2}$ is related to the same discontinuity near the exit of the air gap.

The terms α_1 and α_2 will be referred to as the penetration angles, in *rad*. They are related to the length of air gap, in the θ coordinate, which is reached by each wave, meaning that the wave $\mathbf{B_1}$ will reach a greater length of the air gap, in the θ coordinate, if α_1 is greater. The same is applicable to the $\mathbf{B_2}$ wave and α_2, however in different directions. Note that the wave $\mathbf{B_1}$ travels in the negative direction of θ, while $\mathbf{B_2}$ travels in the positive direction of θ.

The term k_e is related to the speed of these end effect waves in the θ coordinate, which can be different from the speed of the travelling wave $\mathbf{B_s}$, related to the electric speed as per $\frac{2\pi f}{k}$. Therefore, the speed of the end effect waves is given by:

$$\omega_e = \frac{2\pi f}{k_e}. \tag{20}$$

3.5. General Solution

The general solution for the equation 7 will be the sum of the steady-state solution and the transient solution:

$$\begin{aligned}\mathbf{B}(t,\theta) =&\overline{B_s}\exp\left[\jmath(\omega t - k\theta)\right]\\ &+\overline{B_1}\exp\left(-\frac{\theta}{\alpha_1}\right)\exp\left[\jmath(\omega t - k_e\theta)\right]\\ &+\overline{B_2'}\exp\left(\frac{\theta}{\alpha_2}\right)\exp\left[\jmath(\omega t + k_e\theta)\right].\end{aligned} \tag{21}$$

This solution represents the magnetic field in the air gap, which is both a function of time and space. The first wave is the travelling wave, which travels in the negative direction of θ. The second wave also travels in the negative direction of θ and is damped by $-\frac{1}{\alpha_1}$. The last wave travels in the positive direction of θ and is damped by $\frac{1}{\alpha_2}$.

Since the wave $\mathbf{B_2}$ is supposed to exist only nearby the exit of the motor, it is advantageous for computer simulations that a new reference for θ is considered for this wave, as using the previous equation would result in overflow due to the positive exponential [7]. Therefore, it is more advantageous to consider the solution as expressed by:

$$\begin{aligned}\mathbf{B}(t,\theta) =&\overline{B_s}\exp\left[\jmath(\omega t - k\theta)\right]\\ &+\overline{B_1}\exp\left(-\frac{\theta}{\alpha_1}\right)\exp\left[\jmath(\omega t - k_e\theta)\right]\\ &+\overline{B_2}\exp\left(\frac{\theta-\beta}{\alpha_2}\right)\exp\left[\jmath(\omega t + k_e(\theta-\beta))\right]\\ =&\mathbf{B_s}+\mathbf{B_1}+\mathbf{B_2}\end{aligned} \tag{22}$$

3.6. Boundary Conditions

In order to find the amplitudes of the end-effect waves $\mathbf{B_1}$ and $\mathbf{B_2}$, the boundary conditions must be found. The basic approach will be to consider that the full length of the air gap in the θ coordinate is under the influence of the primary current density $\mathbf{j_1}$. Another condition can be found if it is considered that fringing occurs at the edges of the motor. Fringing can be described as the existence of magnetic field outside of the air gap, in the vicinity of the entry and exit ends of the motor. This is in accordance to the model explained by Duncan [6]. The simplest approach for the definition of the boundary conditions is to consider a small angle ξ in which the magnetic field exists outside the air gap, as per figure 6, and apply the magnetic flux conservation:

$$\int_{-\xi}^{\beta+\xi}(\mathbf{B_s}+\mathbf{B_1}+\mathbf{B_2})d\theta = 0. \tag{23}$$

If a small domain on the surface of the rotor not under the air gap is considered, it should not be under the influence of any current or magnetic field. As this domain enters the zone under the air gap, it will be subject to a big variation of the magnetic flux. Therefore, another good approximation would be to consider that, near the entry and exit ends of the motor, $\frac{\partial}{\partial\theta} \gg \frac{\partial}{\partial t}$.

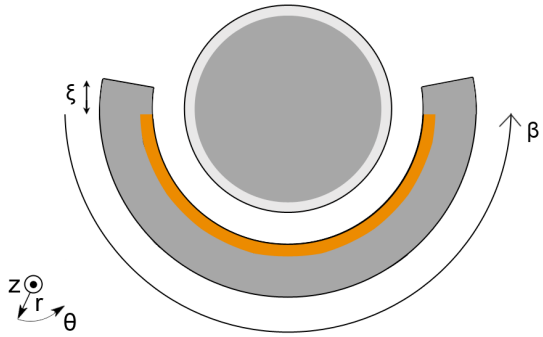

Figure 6: Boundary conditions, considering a ξ angle with no primary winding.

4. Model Analysis

The terms α_1, α_2 and k_e are the most relevant for understanding the way the proposed model is affected by motor parameters and how it influences the actual end effects and motor performance.

Frequency f	50 Hz
Number of pole-pairs k	2
Primary sheet width d_s	1 mm
Secondary sheet width d_r	1 mm
Rotor radius r_r	135 mm
Air gap length g	3 mm
Stator angle β	π rad
Secondary sheet resistivity ρ_s	2.6497x10^{-5} Ω
Primary current density J_M	5.5x10^6 A/m

Table 1: Motor parameters used for model's parameters' plots.

Using the motor parameters of table 1, variation of term α_1 has been plotted in figure 7. The most interesting phenomenon occurring is the shift in behaviour of α_1 between low and high speeds. For high speeds, a larger air gap results in a smaller α_1, but for lower speeds, a smaller air gap results in a smaller α_1. This behaviour has been verified in linear induction motors [3], and is used to categorize motors by low and high speed.

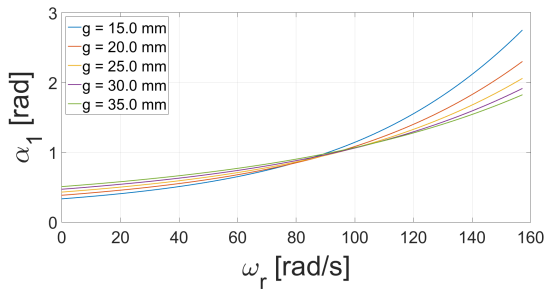

Figure 7: α_1 for various air gaps.

The term α_2 does not show a shift in behaviour, and it is generally of much smaller magnitude than α_1, as was expected and proved in linear induction motors [3], [7].

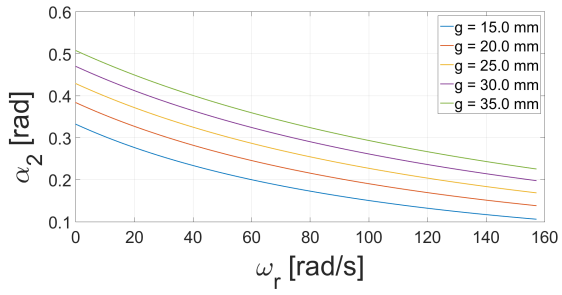

Figure 8: α_2 for various air gaps.

As for the term k_e, some additional notes have to be made. It is not interesting to plot k_e but rather the speed of the end effect waves, ω_e, which depends on k_e.

A new term γ can be defined to identify the zone where α_1 shifts its behaviour, being therefore associated with the separation between low and high speed motors.

$$\gamma = \frac{r_g r_r \mu_0 \omega_r^2}{4\omega\rho_s} \tag{24}$$

For high speed motors, ω_r is very large, and hence some simplifications of the model's parameters can be made for this case. These result in:

$$k_e = \frac{Y}{2} = \frac{k}{1-s} \tag{25}$$

and

$$\omega_e = \frac{2\pi f}{k_e} = \frac{2\pi f(1-s)}{k} = \omega_r. \tag{26}$$

Therefore, if motor speed is high enough, for high speed motors, the end effect waves' speed ω_e becomes the motor speed ω_r. This can be verified with the plot of ω_e for varying air gaps.

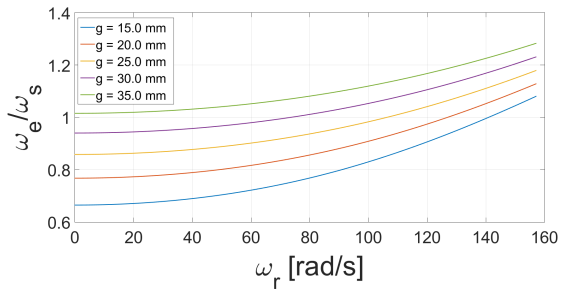

Figure 9: ω_e for various air gaps.

Now, it is clear that once the speed of the motor becomes high enough, the speed of the end effect waves becomes the same as the motor speed. This can be observed running the previous tests for a high speed motor, as seen in figure 10.

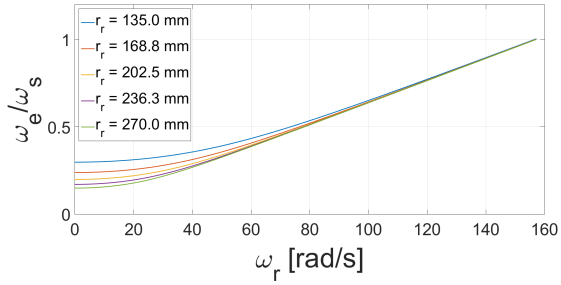

Figure 10: ω_e for various rotor radiuses.

The parameter $\gamma = 22.6$ for the last $r_r = 270mm$ and $\omega_r = 157rad/s$, which means that the motor can be considered to be a high speed motor, under those specifications.

The impact of the end effects is not clear in terms of its influence on motor performance. Hence, motor thrust has been plotted and the analytical expressions have been obtained. Two curves are plotted: the first curve is considering only the magnetic field $\mathbf{B_S}$ due to the primary windings, while the second curve is considering both $\mathbf{B_S}$ and $\mathbf{B_1}$.

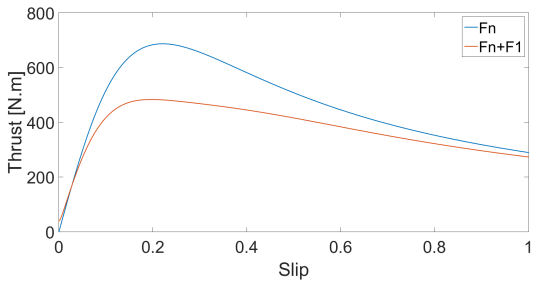

Figure 11: Thrust curves for a low speed motor.

It is evident that the end effect waves reduce thrust for most of the slips. However, some interest-

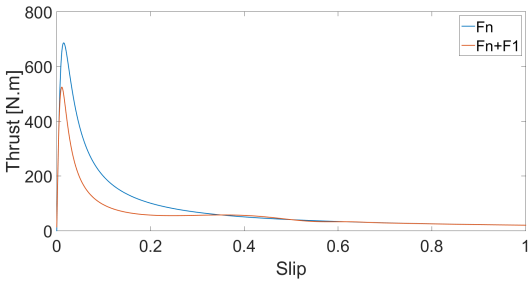

Figure 12: Thrust curves for a high speed motor.

ing phenomenons occur. For low speed motors, it is observed that thrust exists for $s = 0$. This is due to the fact that the term $\frac{\omega_e}{\omega_r}$ is not equal to 1 for low speeds, and hence there is a difference in speeds between the travelling wave and the end effect waves. This means that some currents are being induced in the secondary due to the end effect waves at $s = 0$, hence creating some thrust.

For high speed motors, an ondulatory thrust can be observed for higher slips. This is due to the position of wave's $\mathbf{B_1}$ phasor, if a moving referential is considered where phasors $\mathbf{B_S}$ and $\mathbf{j_1}$ move at speed ω_s. As the end effects speed ω_e is very close to the motor speed ω_r, wave's $\mathbf{B_1}$ phasor is moving very slightly relative to $\mathbf{j_1}$, which can be considered a static phasor. Hence, once wave's $\mathbf{B_1}$ phasor enters the left side plane, negative thrust is generated, and when it enters the right side plane, positive thrust is generated.

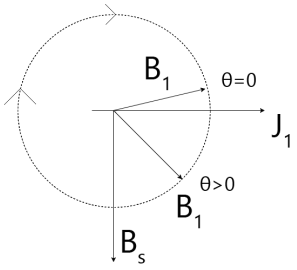

Figure 13: $\mathbf{B_1}$ phasors representation for a high speed motor, at $s \neq 0$.

5. Results

5.1. Finite Element Analysis Simulations

Using a Finite Element Analysis software, a model sharing the same geometric characteristics as the ones in table 1 was created and simulated for various slips over time. The grid frequency was however changed to $f = 10Hz$ in order to reduce simulation times. The resulting magnetic field inside the air gap was obtained, and is shown in figures 14, 15, 16 and 17.

Already, it can be seen that the magnetic field does indeed have a complicated profile inside the

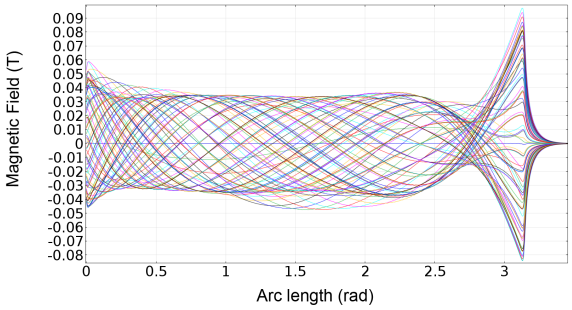

Figure 14: Finite Element Analysis simulation for $s = 1$.

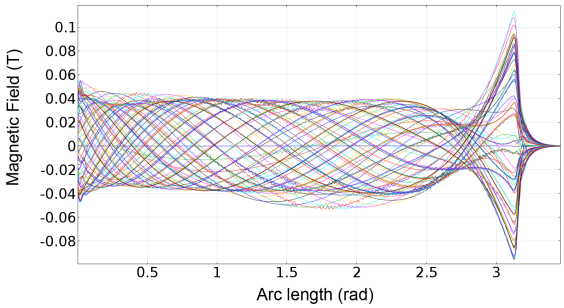

Figure 15: Finite Element Analysis simulation for $s = 0.9$.

air gap. For high slips, for most of the air gap, the magnetic field seems to be close to the travelling wave alone, except for near the extremities of the motor. In the entry end, which is on the left side of the figures, magnetic field seems to increase. This however does not go against the theory regarding the dynamic end effects, since for high slip, the motor can be considered stationary, under little effect of the dynamic end effects and as such were not included in that analysis. However, it can be explained as the amplitude of wave $\mathbf{B_1}$ being larger than the amplitude of wave $\mathbf{B_S}$ for high slips.

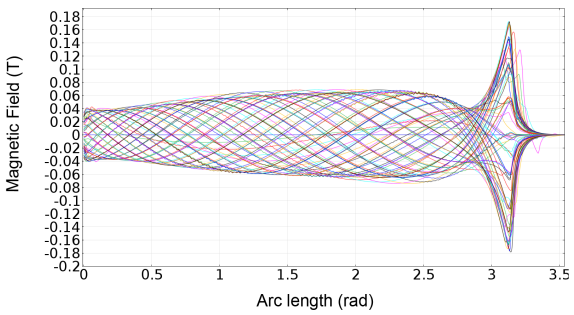

Figure 16: Finite Element Analysis simulation for $s = 0.5$.

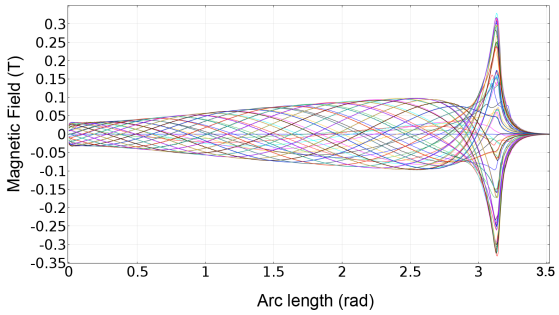

Figure 17: Finite Element Analysis simulation for $s = 0.1$.

Another interesting note for analysis is the funneling of magnetic field that seems to occur for any slip, near the exit end, corresponding to the right side of the figures. This point can be explained if the two waves that make up the proposed model are remembered, as one travel in one direction and the other in the opposite direction, which different attenuation constants. This funnel point is where the exit end effect wave starts influencing the magnetic field. Since its damping constant is very small, its impact is reduced to a very limited arc length near the exit, therefore creating a very sudden increase in the magnetic field.

For low slips the magnetic field seems to correspond almost exactly to what was expected in theory. In the entry end, a reduced magnetic field is obtained, while near the exit end it is increased substantially.

5.2. Proposed Model Simulations

A value for ξ must be estimated, according to the set of boundary conditions proposed. Various simulations were tested and the value that seemed to result in a closer profile to the Finite Element Analysis software was $\xi = 0.0483$. Note that this value for ξ should only be used as an approximation for these motor specifications, as per table 1.

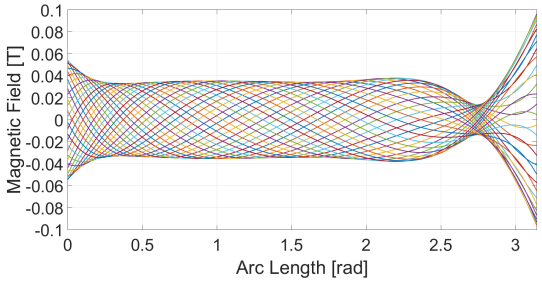

Figure 18: Model simulation for $s = 1$.

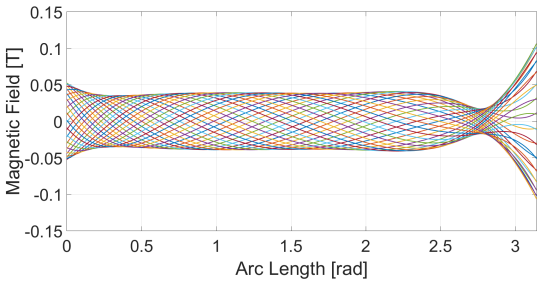

Figure 19: Model simulation for $s = 0.9$.

For high slips, comparing figures 18 and 19 to figures 14 and 15, it seems that the boundary conditions accurately describe the magnetic field profile. It is for lower slips, and hence higher motor speeds, that the set of boundary conditions will be put to test, as impact of the dynamic end effects on motor performance increases.

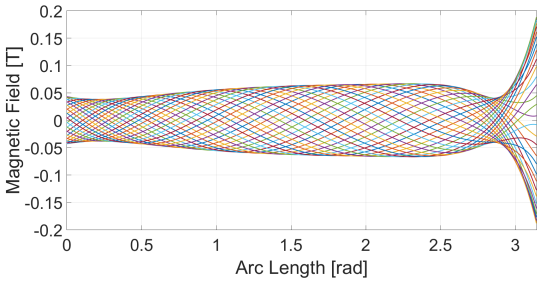

Figure 20: Model simulation for $s = 0.5$.

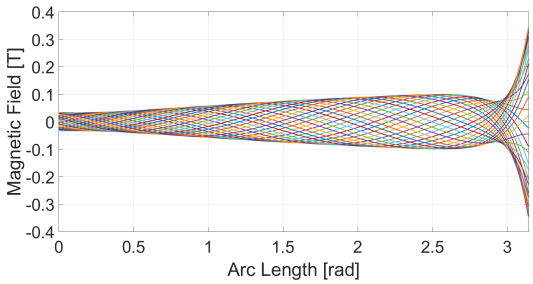

Figure 21: Model simulation for $s = 0.1$.

As observed in figures 20 and 21, compared to 16 and 17, there is a high degree of similarity. The conditions provide a very accurate representation of the magnetic field inside the air gap for all slips.

The set of boundary conditions can be applied to fully describe the profile of the magnetic field inside the air gap for any motor parameters, remaining inside the initial assumptions such as small air gap. The ξ parameter, however, is chosen somewhat arbitrarily and should depend on the motor's parameters, being based upon the results provided by the Finite Element Analysis software.

6. Conclusions

This work proposes a one dimensional model based on the Field Theory to describe the magnetic field inside a spherical induction motor with shell-like stator. The model uses the as basis the linear induction motor models for end effects, and it accurately corresponds to simulations produced by the Finite Element Analysis software. The motor's properties on the model's parameters were studied and can serve as a basis for design of this type of motor, in order to reduce the effect of the end effects on motor performance.

The one dimensional model was presented through analysis of the electromagnetic laws. Some approximations were made, including the non variation of the magnetic field in the θ coordinate, a small air gap and equivalent conductive sheets for the primary winding and the secondary sheet. These approximations are based on previous work in linear induction motors' analysis through Field Theory, such as in references [3] and [7]. The resulting model produces two end effects waves, $\mathbf{B_1}$ and $\mathbf{B_2}$, which can be thought of as the entry end effect wave and the exit end effect wave, correspondingly, which, in conjunction with the travelling wave $\mathbf{B_S}$ translate the profile of the magnetic field inside the air gap. These end effect waves travel in opposite directions in terms of the θ coordinate, and have different damping constants α_1 and α_2.

A set of boundary conditions had to be found, where a small angle ξ outside of the air gap was considered, in which magnetic field and induced currents could exist. This ξ angle is arbitrary, and only with the help of the Finite Element Analysis software results was it possible to estimate a value for it. After achieving a value that corresponded to the Finite Element Analysis software, all the simulations made with the same ξ seemed to correspond to the Finite Element Analysis software simulations.

The obtained parameters of the model were discussed and their sensitivity to the motor physical properties was analysed. Some interesting points were made, specifically regarding the difference between high speed and low speed motors, as the model's parameters seem to have a complete opposite behaviour from a certain undefined point in terms of motor speed. This undefined point, or rather undefined area, can be estimated through the γ parameter found, which depends on the motor's physical properties such as radius and secondary sheet conductivity. The biggest conclusion in this section is the difference between the penetration depths α_1 and α_2, which defined the damping of the end effect waves as they travel through the θ coordinate. It was found that α_1 is generally much larger than α_2, hence wave $\mathbf{B_1}$ should have a much larger contribution of the distortion of the magnetic field inside the air gap than wave $\mathbf{B_2}$. This corresponds to the previous work done on the linear induction motor as well.

Lastly, various simulations were made in the Finite Element Analysis software in order to validate the proposed model. Three stator angles were chosen and various different slips were used. The set of boundary conditions seem to be in total accordance to the Finite Element Analysis software, particularly in the entry and exit ends of the motor.

The model, with the specified set of boundary conditions, explains the complicated profile of magnetic field found inside the air gap.

References

[1] João F. P. Fernandes, P. J. Costa Branco. The shell-like spherical induction motor for low-speed traction: Electromagnetic design, analysis and experimental tests. *IEEE Transactions on Industrial Electronics*, 2015.

[2] Klemens Kahlen. Torque control of a spherical machine with variable pole pitch. *IEEE Transactions on Power Electronics*, 2004.

[3] Sake Yamamura. *Theory of Linear Induction Motors*. Halsted, 1972. ISBN: 0-470-97090-1.

[4] E. Amiri, E. Mendrela. *Induction Motors with Rotor Helical Motion*. InTech, 2012. ISBN: 978-953-0843-6.

[5] H. Tiegna, Y. Amara, G. Barakat. Overview of analytical models of permanent magnet electrical machines for analysis and design purposes. *Elsevier B.V*, 2013.

[6] J. Duncan. Linear induction motor-equivalent-circuit model. *IEEE Transactions on Industrial Electronics*, 1983.

[7] Michel Poloujadoff. *The Theory of Linear Induction Machinery*. Clarendon, 1972. ISBN: 0-19-959322-8.

[8] Carlos Manuel Pereira Cabrita. *Motor Linear de Indução - Análise Teórica, Projecto e Ensaio*. PhD thesis, Instituto Superior Técnico, 1988.